Morphology, Dispersion, and Stability of Cu Nanoclusters on Clean and Hydroxylated α-Al_2O_3(0001) Substrates

M. C. R. Jensen,[†] K. Venkataramani,[†] S. Helveg,[‡] B. S. Clausen,[‡] M. Reichling,[§] F. Besenbacher,[†] and J. V. Lauritsen*,[†]

Interdisciplinary Nanoscience Center and Department of Physics, University of Aarhus, Denmark, Haldor Topsøe A/S, Denmark, and Department of Physics, University of Osnabrück, Germany

Received: May 21, 2008; Revised Manuscript Received: September 01, 2008

Using high-resolution dynamic scanning force microscopy (SFM) operated in the noncontact mode, we investigate here the detailed morphology, dispersion, and thermal stability of nanometer-sized three-dimensional Cu clusters on an α-Al_2O_3(0001) substrate. We systematically study the effect of surface hydroxylation by depositing metallic Cu either on an ultrahigh vacuum prepared Al-terminated alumina surface or on surfaces prehydroxylated/hydrated by exposure to varying doses of H_2O. Three-dimensional growth of Cu nanoclusters dispersed evenly on the surface is observed independent of surface preparation. As the top facet of the nanoclusters appears hexagonal in SFM images, we conclude that they are regular Cu crystallites in the equilibrium form. For strongly hydroxylated surfaces, however, a reduced aspect ratio (height-to-width) of the nanoclusters indicates an increased wetting of the Cu. We propose that Cu bonding to the hydroxylated surface is enhanced by the formation of Cu−O−Al bonds. Surprisingly when heating the surface, Cu remains dispersed on the surface, but it is observed that the total coverage of Cu on the surface is rapidly reduced when the sample is heated to temperatures above 450 °C for clean and 550 °C for hydroxylated surfaces. Our results unexpectedly show that Cu is desorbed from the ~3 nm wide Cu nanoclusters at temperatures well-below the melting temperature of bulk Cu, and the sublimation is completed before the onset of sintering or ripening of the Cu nanoclusters under the conditions of our experiment. Our observations thus reveal significant changes in the cohesive energies of nanometer-sized Cu clusters, which is an effect that should be taken into account when modeling the stability of Cu crystallites, for example, with regard to sintering of Cu-based catalysts.

I. Introduction

The majority of industrial heterogeneous catalysts employ porous metal oxides as a material serving in different functions.[1,2] Mostly, the role of the porous metal oxide is that of a passive support dispersing the active metallic component into nanocrystals to facilitate contact with the gaseous reactants. The ability to control and stabilize the dispersion of metal nanoclusters on metal oxides is crucial for the activity and selectivity of most heterogeneous catalysts, in particular, since the highly dispersed state of nanoclusters is energetically unfavorable compared with the agglomerated state, and sintering is therefore a common cause of activity decline in catalysts. In this context, a clear understanding of the nature of the interface between metal nanoclusters and metal oxides is crucial in order to model sintering and eventually prevent catalyst deactivation. Furthermore, there are prominent examples where the oxide support plays an active role in the catalytic process either in synergy with a dispersed phase in a bifunctional catalytic mechanism (e.g., in hydrocracking[3]), by spill-over reactions, by supporting special or dynamic nanocluster morphologies,[4,5] or by generating favorable catalytically active sites at the cluster/oxide interface.[6,7] In many cases, however, detailed experimental insight into metal nanoclusters supported on metal oxides has been quite difficult to obtain since most relevant metal oxides are insulating and hence difficult to study due to charging problems in traditional surface science techniques. A further complication is related to the fact that the atomic surface structure of metal oxide supported nanoclusters is not readily accessible. Scanning tunneling microscopy (STM) has recently demonstrated its great value in the characterization of nanoclusters on conducting substrates as models of catalysts. For the range of insulating metal oxides (e.g., Al_2O_3 or MgO), a useful trick is to synthesize thin films on metallic substrates, which enables tunneling through the substrate.[8−10] However, recent theoretical studies have pointed out that electronic coupling to the metallic substrate may stabilize metal-oxide structures different from any known bulk structure,[11−13] and therefore, the surface of the thin film may not be a generally valid model for the surface of a bulk oxide. Detailed surface science studies of nanoclusters on real bulk insulating metal-oxide surfaces, such as alumina (Al_2O_3), are very scarce because of technical difficulties in preparing and characterizing insulator surfaces. However, owing to recent developments in dynamic mode scanning force microscopy (SFM), which may provide direct-space atom-resolved images of surfaces and nanostructures independent of the surface conductivity,[14] such insight is now within reach for clusters and nanostructures supported on insulator substrates.[15−18]

In the present paper, we use SFM to study the Cu/Al_2O_3 system, which is of considerable fundamental interest, for example, because of its use in catalysts for large-scale commercial processes such as the methanol synthesis and low-temperature water−gas shift reaction. Moreover, the system has

* Corresponding author. E-mail: jvang@inano.dk.
[†] University of Aarhus.
[‡] Haldor Topsøe A/S.
[§] University of Osnabrück.

10.1021/jp804492h CCC: $40.75
Published on Web 10/02/2008

also recently demonstrated promising results for low-temperature water−gas shift application in mobile fuel cells.[19] In methanol synthesis, the ternary $Cu/ZnO/Al_2O_3$ catalyst exhibits a higher catalytic activity than each of the separate Cu/ZnO or Cu/Al_2O_3 systems, but the exact synergetic effects between these materials are still under intense debate.[20−22] Traditionally, the role of the Al_2O_3 is considered to act as a stabilizer for the Cu nanoclusters and prevent rapid sintering of Cu particles, but the fundamental interaction between Cu and Al_2O_3 still remains to be clarified. A key question in this regard seems to be the stability of Cu nanoclusters when the system is exposed to water, since the catalytic activity and sintering resistance have been observed to depend on the accumulated effect of exposure to water.[20] However, a clear understanding of the role of water in this system and a general atomic-scale understanding of the nature of Cu bonding to clean and hydrated alumina surfaces is far from established. Our strategy in this paper utilizes high-resolution SFM to systematically study the thermal stability and morphology of Cu nanoclusters deposited on ultrahigh vacuum (UHV)-prepared clean α-$Al_2O_3(0001)$ as well as hydroxylated Al_2O_3 substrates prepared by pre-exposure to varying fluxes of water. The detailed insight into the cluster morphology obtained from SFM experiments is important, since it makes it possible to extract information on the cluster−interface adhesion energies, the so-called work of adhesion (W_{adh}).[23,24] The adhesion energy of a Cu nanocluster is dependent on the exact composition and structure of the interface between the cluster and the substrate, and previous studies have specifically shown that the adhesion of metals on Al_2O_3 may change with the density of surface hydroxyls.[25−27] In the case of Cu deposited on the hydroxylated Al_2O_3, an exchange reaction between H from an terminal hydroxyl (H−O−Al) and deposited Cu has been proposed from theory leading to rather strong Cu−O−Al bonds and hence a large W_{adh}.[28] However, $Al_2O_3(0001)$ surfaces are known to adopt many different terminations depending on the preparation route and environment conditions.[29] In order to systematically investigate the influence of water on the Cu adhesion, we have therefore prepared surfaces with varying degrees of surface hydroxyl groups and studied the morphology of Cu nanoclusters. Using values extracted from a detailed characterization of the width, height, and morphology in SFM images of hexagonally shaped Cu nanoclusters, we performed a quantitative calculation of the Cu−substrate adhesion energies based on the Wulff construction for supported nanoparticles[30,31] and show that the adhesion of Cu below 300 °C is significantly influenced by hydroxylation of Al_2O_3. At subsequent higher temperatures up to 600 °C, SFM images reveal that the hydroxylation level of the Al_2O_3 surface gradually decreases because of desorption, and accordingly, hydroxylation has less impact on the cluster morphology. Instead, we observe a large loss of Cu present on the surface at temperatures exceeding 500 °C, which is attributed to desorption of Cu.

II. Experimental Section

The experiments were performed in an ultrahigh vacuum (UHV) chamber with a base pressure of 1×10^{-10} mbar. The chamber was equipped with an SFM (Omicron VT-SFM) enhanced with an EasyPLL-plus electronics (Nanosurf AG). SFM measurements were performed in the noncontact mode of operation (nc-SFM)[14] using commercial cantilevers with a nominal tip radius smaller than 2 nm (SuperSharpSilicon-NCH from Nanosensors). In the noncontact mode, exclusively attractive forces active at the onset of bonding between atoms of the tip apex and surface atoms are probed. Topographic images were recorded by oscillating the SFM cantilever at its resonance frequency (~300 kHz) with a stabilized amplitude of 20 nm (peak-to-peak) and recording the frequency shift (*df*) induced by the interaction force as a feedback to control the tip−surface distance during scanning.

The sample was a polished α-$Al_2O_3(0001)$ crystal (MTI Corporation, USA) cleaned ex-situ in 35% HNO_3 for 30 min, rinsed in water, and annealed for 8 h at 1200 °C under atmospheric conditions. Subsequently and for each new Cu deposition, the sample underwent multiple ion-sputtering (15 min, 1.5 keV, Ar^+) and annealing cycles (1200 °C) in oxygen (10^{-7} mbar). The sample temperature was monitored directly on the front of the crystal using an optical pyrometer (Metis MY81, Sensortherm GmbH), which was precalibrated against a K-type thermocouple reading in direct contact with the crystal. With atom-resolved SFM,[32] we determined the surface structure of the α-$Al_2O_3(0001)$ to be the well-known $\sqrt{31} \times \sqrt{31}R \pm 9°$ reconstruction[33−35] (see e.g. Figure 1a). In accordance with previous results,[33,36] the $\sqrt{31} \times \sqrt{31}R \pm 9°$ reconstruction was not lifted by exposing it to oxygen at moderate pressures ($<1 \times 10^{-7}$ mbar) even at high temperatures (>1000 °C), but we used oxygen treatments for our sample preparation anyway since it had a very beneficial effect on the surface flatness.[35] The surface structure and cleanliness were monitored by atom-resolved SFM and X-ray photoelectron spectroscopy (XPS) using unmonochromatized Mg Kα radiation (Phoibos 100 analyzer SPECS GmbH, Germany). Figure 2a shows an XPS survey spectrum of the Cu deposited surface. In the XPS spectra acquired throughout the studies, only peaks belonging to Al and O and the deposited Cu were observed. Partially hydroxylated surfaces such as those introduced in ref 37 were prepared by exposing the freshly prepared sample to triply distilled water in the UHV chamber dosed through a UHV leak valve. The water was purified by several freeze−pump−thaw cycles. Higher degrees of hydroxylation require exposure to much higher partial pressures of water,[26,36] and to accomplish this, the sample was transferred to a small evacuated cell and exposed to pure water vapor (~5 min) from a reservoir at its ambient partial pressure at room temperature (~ 25 mbar at 21 °C). After water exposure, the cell was evacuated, and the hydroxylated sample was transferred back to the UHV chamber for Cu deposition and SFM analysis. Cu was deposited under vacuum conditions ($\sim 2 \times 10^{-10}$ mbar) onto the substrate from an e-beam evaporator (flux ~ 0.04 ML/min). The flux setting of the e-beam evaporator was set to this value prior to dosage, and the dose rate was kept constant for all experiments. The total Cu coverage was subsequently estimated from a measurement of the total Cu volume seen in the SFM images taken after room temperature deposition and was found to be 0.25 ± 0.05 monolayer (ML), where 1 ML is defined as the two-dimensional (2D) packing density of copper $\sim 1.77 \times 10^{15}$ atoms/cm^2. We observed a slight charging of the substrate after Cu deposition detected by a rise in surface potential to ~3−5 V, which was detected by the SFM. The surface charging, which is in general unwanted for high-resolution SFM, could be eliminated by exposing the sample front to a short pulse (3−7 s, 0.2 mA emission) from an electron flood gun providing electrons with energy of about 2 eV. Remaining potential differences between tip and sample could be fully compensated by adjusting the bias voltage applied between the tip and the metallic sample support as described in previous work.[59]

III. Results and Discussion

A. Cu Nanoclusters on α-$Al_2O_3(0001)$. Figure 1a,b illustrates high-resolution SFM images of the α-$Al_2O_3(0001)$

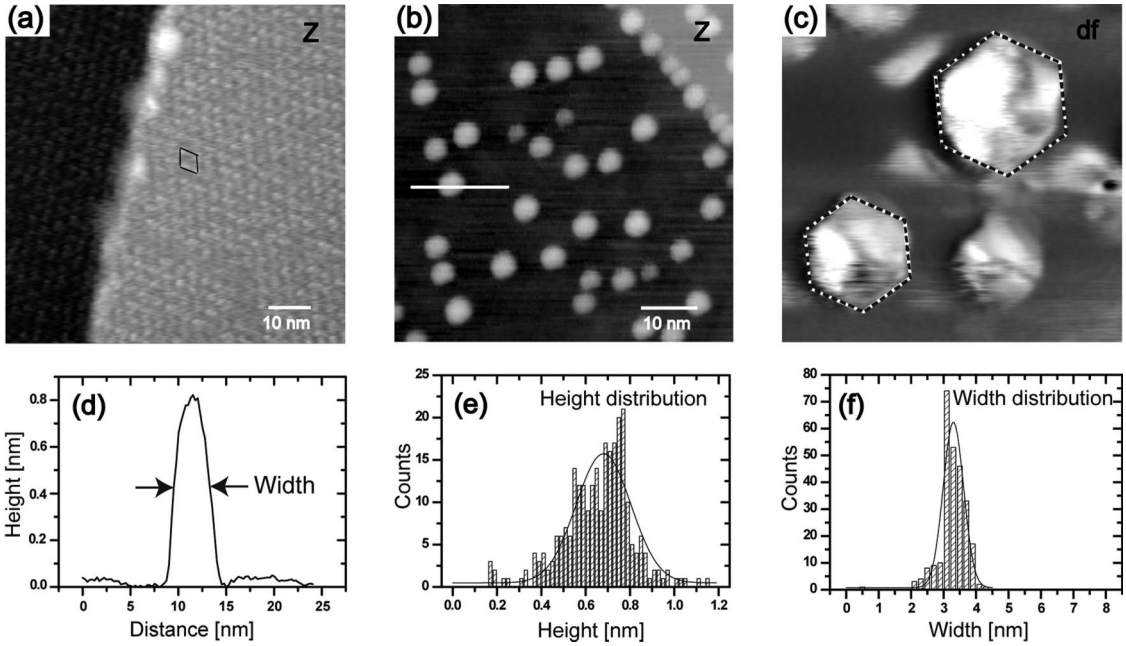

Figure 1. (a) Topographic SFM image of the clean α-Al_2O_3(0001) in the reconstructed state. (b) Topographic SFM image after deposition of 0.25 ML Cu and postannealing to 300 °C. (c) A zoom-in constant height SFM image (35 nm × 35 nm) ($df_{set} = -23$ Hz). (d) The graph illustrates a cross section profile of a nanocluster in the topographic image. (e) Height histogram of Cu nanoclusters. (f) Corresponding width histogram. A Gaussian fit to the distributions is shown as a solid line.

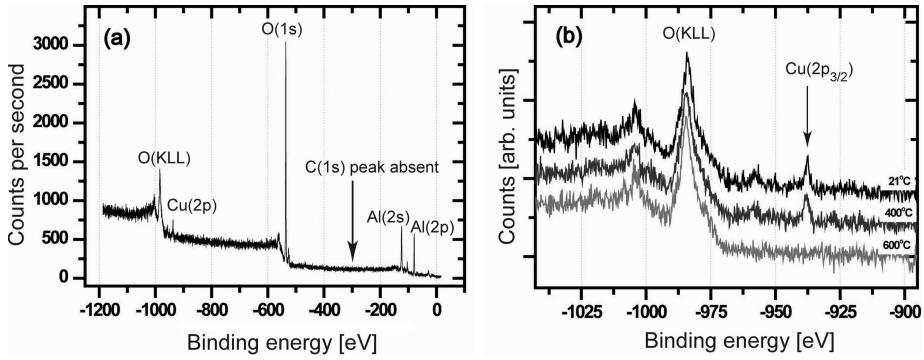

Figure 2. (a) XPS survey scan of the α-Al_2O_3(0001) surface taken at room temperature immediately after Cu deposition. (b) O(KLL) and Cu($2p_{3/2}$) signal recorded at room temperature (21 °C) and after heating the sample to 400 and 600 °C, respectively.

before and after Cu deposition. In Figure 1b, the deposited Cu is observed to be dispersed on the surface in the form of three-dimensional nanometer-sized clusters, indicating a Volmer−Weber growth mechanism of Cu on Al_2O_3(0001) in agreement with earlier studies.[8,15] The nucleation of Cu nanoclusters is observed on both the (0001) terrace planes and the upper rim of step edges. In order to ensure that the nanoclusters imaged by SFM reflect an equilibrium morphology and not a kinetically limited structure, we performed sequential postdeposition heating of the Cu deposited surface and characterized the cluster morphology and shape. After postannealing at temperatures in the 100−300 °C regime, we find that the cluster density, size, and shape remained unaltered, indicating that nanoclusters formed under these conditions reflect an equilibrium structure. It should be noted that tip-convolution (broadening) effects may be pronounced in SFM studies, and the cluster dimensions estimated from SFM in general represent an upper limit to the real value. For the same reasons, it has proven to be very difficult to resolve the exact shape of nanoclusters in regular topographic SFM images in previous studies. However, as shown in Figure 1c, it was possible to directly resolve the shape of the top facet of the Cu nanoclusters with the SFM. As recently demonstrated in ref 18 and explained in ref 38, tip convolution effects may be significantly reduced in images representing the SFM detuning signal (*df*) recorded by scanning in the constant height mode in contrast to the topographic images produced from scanning in the constant detuning mode. It is apparent from our constant height SFM image in Figure 1c that the top facet of the Cu nanoclusters is preferentially shaped as a regular hexagon, suggesting that this shape reflects the equilibrated form of Cu nanocrystallites oriented with the (111) facet toward the Al_2O_3(0001) surface. Our observations are supported by the fact that the same regular hexagonal shape of the top facet was resolved for Cu nanoclusters grown on a Al_2O_3-like thin film in a previous STM study by Worren et al., where atom-resolved STM furthermore showed that such nanoclusters expose an unreconstructed (111) facet of Cu on the hexagonal top facet.[8]

The exact equilibrium morphology of the Cu nanoclusters in Figure 1b,c is in principle determined by the relative free energies of the cluster facets and the interfacial energy. In terms of the Wulff construction[30] for supported clusters, it is possible to use the observed parameters for the morphology to directly extract approximate values for W_{adh}. The formal procedure is described in detail in refs 8 and 9. Since the observed shape of the Cu nanoclusters in this paper is very similar to those in ref 8, we will assume that the hexagonal top facet is a (111) plane

of Cu, and we use the formal framework of the latter paper for the interpretation of our data. The work of adhesion is given by the following expression:

$$W_{adh} = 2\gamma_{111} - \frac{h}{l_{111}}\left(-\frac{3}{\sqrt{2}}\gamma_{111} + \sqrt{3}\gamma_{110} + \sqrt{\frac{3}{2}}\gamma_{100}\right) \quad (1)$$

where the γ are the surface free energies of Cu low index facets, h is the height, and l_{111} is the exact width of the hexagonal top facet. In the limit of small clusters where the (110) facet is not developed, the expression changes to[39]

$$W_{adh} = 2\gamma_{111} - \sqrt{\frac{3}{2}}\frac{h}{l_{111}}\gamma_{100} \quad (2)$$

In order to estimate the input parameters, we have characterized the width and height of the Cu nanoclusters in a large number of high-resolution topographic SFM images. The cluster width was estimated from line scans performed across the nanoclusters by measuring the full width at half-maximum, as illustrated in Figure 1d. The height was correspondingly measured as the height difference between the cluster top facet and the flat substrate. Figure 1e,f shows the distribution of the cluster height and width obtained for the whole ensemble of nanoclusters. The most frequently observed values for the cluster height and width and the respective standard deviations were then obtained as the average value and variation from the respective Gaussian fits. The most frequent Cu nanocluster width and height were found to be 3.2 ± 0.3 nm and 0.7 ± 0.1 nm, respectively, revealing the formation of rather wide nanoclusters with 3−4 atomic layers of Cu on the Al_2O_3 surface on average. The cluster width of 3.2 nm is according to Worren et al.[8] below the threshold at which (110) start to develop on the clusters, and accordingly, we will use eq 2 to calculate W_{adh}. Approximating the respective h and l_{111} values to the most frequent height and width measured with SFM and using the most recent theoretical literature γ values of Cu,[40] we calculate W_{adh} to be 3.32 ± 0.13 J/m^2 on the clean Al_2O_3 surface. The type of bonding reflected by this work of adhesion value at the interface between the Cu nanoclusters and the $Al_2O_3(0001)$ is considered to be metallic and not oxidic, since the $Al_2O_3(0001)$ surface prepared by annealing to high temperatures (<1000 °C) under UHV exposes the so-called $\sqrt{31} \times \sqrt{31}$R° ± 9 reconstruction. This is illustrated in Figure 1a, where the hexagonal pattern of protrusions resolved in the SFM images with a periodicity of 2.65 nm is a reflection of the $\sqrt{31} \times \sqrt{31}$R ± 9° reconstruction of α-$Al_2O_3(0001)$, which was also previously observed by SFM.[35,41] This complex and extraordinarily stable surface reconstruction of Al_2O_3 forms as a consequence of high annealing temperatures, which are necessary to prepare a well-ordered, flat, and clean substrate, and it has been examined in some detail previously.[33,34,42] A detailed atomistic structural model of the $\sqrt{31} \times \sqrt{31}$R° ± 9 reconstruction is not available. However, it is generally believed that the surface layer is completely oxygen depleted relative to the most stable regular (1 × 1) $Al_2O_3(0001)$ termination which exposes both Al and O in the relaxed top layer.[43,44] We adopt this model and anticipate that, on such an Al rich surface, the interaction of Cu with the clean surface is dominated by direct Cu−Al interactions. In support of this, we note that the experimentally estimated value for the W_{adh} is in close agreement with the theoretical estimate by Lodziana et al.[45] who calculated the work of adhesion for Cu on $Al_2O_3(0001)$ surfaces of different stoichiometries with respect to Al and O. When we compare our results with the most Al rich surface, the so-called Al−Al terminated surface, which is obtained by cleaving the R−O−Al−Al−R repetition unit of Al_2O_3 between the oxygen and the double Al layers, a $W_{adh} = 3.26$ J/m^2 was calculated for Cu which is in agreement with the estimate in our experiment. A systematic overestimation of the cluster top facet (l_{111}) of 20% (which is probably realistic for topographic SFM images of clusters due to tip broadening) will not reduce W_{adh} by more than 4.9%, which is still in good agreement with the theory.

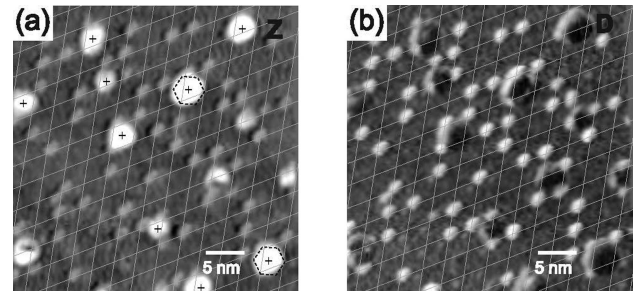

Figure 3. High-resolution SFM images of Cu nanoclusters on the partially hydroxylated surface representing (a) the topography (Z) and (b) dissipation (D) signal. Crosses indicate the center-of-mass for the Cu nanoclusters. Smaller patches defining the rhombic grid are attributed to groups of surface hydroxyls.

B. Cu Nanoclusters on Partially Hydroxylated α-$Al_2O_3(0001)$. A stronger binding to a hydroxylated substrate compared with that to the clean Al_2O_3, that is, a higher work of adhesion (W_{adh}), would be manifested by a change in the equilibrium cluster morphology, and in order to investigate whether such an effect is present for the Cu/Al_2O_3 system, we performed SFM characterization of Cu nanoclusters on prehydroxylated surfaces. It has previously been demonstrated by high-resolution SFM studies by Barth et al.[41,46] that the reorganization of Al atoms within the large $\sqrt{31} \times \sqrt{31}$R° ± 9 unit cell on $Al_2O_3(0001)$ (Figure 1a) lead to a template grid with a spatially modulated affinity toward water adsorption, and more specifically isolated patches of brighter contrast were observed by SFM and tentatively attributed to groups of hydroxyls or very small aluminum hydroxide ($Al(OH)_3$) or oxyhydroxide (AlOOH) nanocrystals formed at certain slightly disordered sites within the unit cell. As shown in Figure 3, we also see by SFM the formation of such groups with brighter contrast in a regular grid determined by the $\sqrt{31} \times \sqrt{31}$R° ± 9 unit cell. Figure 3a,b respectively shows the topography image (Z) and a so-called dissipation signal image (D) recorded simultaneously as a passive signal[14] of a mildly hydroxylated surface resulting from the adsorption of water from the background pressure in the UHV chamber ($P \sim 2 \times 10^{-10}$ mbar). The dissipation signal reflects the energy losses due to hysteresis during the SFM cantilever oscillation cycle and is considered to give a very strong contrast at an adsorbate site, such as a surface OH group, with a high degree of vibrational freedom.[47] On the contrary, rigid structures such as Cu nanocrystals are not expected to give a strong dissipation signal, which is in qualitative accordance with the dissipation image in Figure 3b. The dissipation image thus shows two chemically different species imaged as larger dark ones belonging to Cu nanoclusters and imaged as smaller bright ones belonging to hydroxyls adsorbed on the surface. By a correlation of the position of the center of mass of the Cu nanocluster and the grid defined by the hydroxyls (see Figure 3a,b), we conclude that Cu seems to nucleate at sites (marked by a black cross in Figure 3a) different from the sites preferred by the hydroxyls (marked by the crossing points of the white grid). Since the UHV-prepared Al_2O_3 surface is presumably Al-terminated, it could be expected

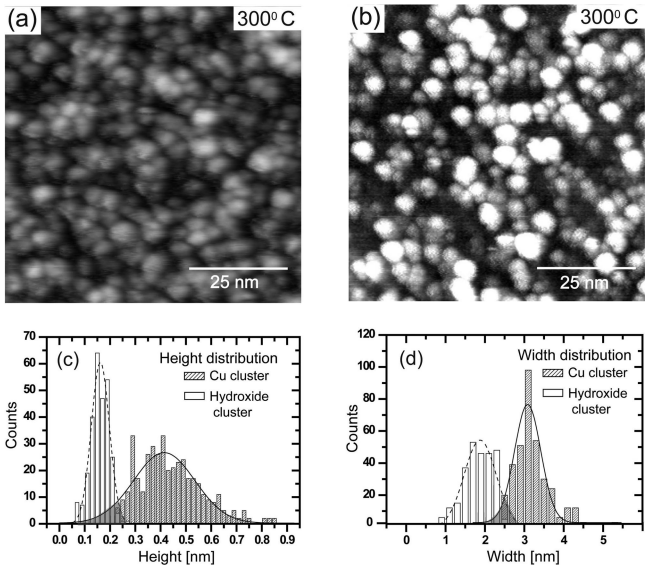

Figure 4. (a) Topographic SFM images of a strongly hydroxylated surface before Cu deposition after a short temperature flash to 200 °C. (b) Topographic image of after Cu deposition, (c) height distribution, and (d) width distribution of AlOOH oxyhydroxide and Cu nanoclusters.

that hydroxylation would change the bonding to Cu by adding oxygen to the surface layer, since Cu−O−Al bonds are generally predicted to be stronger than Cu−Al bonds,[45] thus leading to increased wetting of the Cu overlayer. However, further SFM experiments performed by prehydroxylating the surface under vacuum conditions (5−50 L of H_2O at 5×10^{-9} mbar) and then depositing Cu again showed that such low degrees of hydroxylation have no effect on the nucleation of Cu nanoclusters. Furthermore, the cluster width and height were found to be the same within the statistical uncertainty as that on a clean surface. We therefore conclude that the presence of hydroxyls at low coverage achieved under vacuum conditions have no significant impact on the Cu nanocluster morphology and dispersion. We note that the apparent saturation coverage of hydroxyls on the surface was always rather low (estimated to less than 0.2 ML), and we could not obtain a strongly hydroxylated surface under vacuum conditions, which is in agreement with previous studies.[36]

C. Cu Nanoclusters on Strongly Hydroxylated α-Al_2O_3(0001). Alumina supports contained under wet impregnation conditions used in catalyst synthesis are considered to expose a hydroxylated surface, and in order to model such a condition, we prepared strongly hydroxylated surfaces by exposing the clean α-Al_2O_3(0001) to pure H_2O at its room temperature vapor pressure (∼25 mbar at 21 °C, 5 min) in a vessel attached to the vacuum system. A similar preparation has previously been reported in an XPS study to result in a significant hydroxylation of the Al_2O_3(0001) surface.[26,36] It was extremely challenging to image the strongly hydroxylated surface in very high resolution with SFM at room temperature, possibly due to a high mobility of molecularly adsorbed water species.[26,36] However, after a short flash of the sample to ∼200−300 °C, it was possible to image the surface and observe the effect of surface hydroxylation by the water vapor in some detail. Figure 4a illustrates an SFM image of the Al_2O_3 surface in the strongly hydroxylated state that we recorded in UHV at room temperature. The SFM image reveals a dramatic change in the surface structure as compared with the clean (Figure 1a) and vacuum hydroxylated surface (Figure 3a) Al_2O_3(0001) substrates, and a significant population of very small clusters is detected on the surface. The small clusters were thoroughly analyzed in the SFM images and were found to adopt heights in the range 0.1−0.2 nm relative to the substrate and a corresponding width of approximately 1.8 nm on average. An XPS survey detected no impurities on the surface which could have been present in the water dosed in the cell. We observe that the "hydroxylated" state of the surface was maintained even after prolonged exposure to the UHV environment and heating to rather high temperatures. Heating of the sample in the strongly "hydroxylated" state in Figure 4a to temperatures higher than 350 °C led to decomposition of the surface clusters, and the surface could then be imaged (not shown) in the same $\sqrt{31} \times \sqrt{31}R \pm 9°$ reconstructed state as prior to water dosage (Figure 1a). A study of the thermal decomposition sequence[48] shows that bulk $Al(OH)_3$ (bayerite or gibbsite) is stable up to ∼100−130 °C after which a hydrothermal transformation occurs to an oxyhydroxide phase (AlOOH), which is stable until approximately 300−400 °C. Given the observed thermal stability interval up to ∼350 °C, we thus attribute the small clusters imaged in Figure 4a to aluminum oxyhydroxide (e.g., AlOOH). We speculate that this hydroxylated phase is initially formed by release of excess Al from the clean Al-rich reconstructed Al_2O_3 surface prepared in UHV and that the AlOOH clusters are supported on a nonreconstructed stoichiometric termination of Al_2O_3(0001), possibly with a significant population of OH groups. In any case, the observations imply that the "hydroxylated" surface in Figure 4a represents a surface with a much higher O−H and O content compared with the clean surface, and we will therefore refer to the surface in this state as "strongly hydroxylated". This change in the surface composition is clearly reflected in the apparent equilibrium morphology of Cu nanoclusters deposited on the strongly hydroxylated surface. Figure 4b shows the hydroxylated surface after Cu deposition using the same parameters as before and a post-heated to 300 °C. A statistical analysis of the cluster width and height is performed similar to Figure 1 to address the effect of hydroxylation on the Cu nanocluster dimensions. To neglect an influence on the Cu nanocluster dimensions by the AlOOH clusters present on the surface, we carefully analyzed the height and width distribution of the oxyhydroxide clusters on a strongly hydroxylated surface before Cu deposition, as a reference. Generally, the oxyhydroxide clusters were much smaller in both width and height, and a comparison of the cluster width and height distribution (Figure 4c,d) obtained for Cu nanoclusters selected from the SFM images shows that the region of overlap is very small, indicating that the values obtained by us are reliable with a high degree of certainty. We can therefore extract the Cu cluster dimensions from the SFM images. For temperatures higher than 350 °C, the oxyhydroxide cluster concentration decreased significantly, thus further reducing the overlap.

As for the analysis on the clean surface, we consider Cu nanoclusters formed after postdeposition heating in the 100−300 °C regime to reflect the equilibrium state. The most frequently observed value for the Cu cluster width was found to be 3.2 ± 0.1 nm, which is similar to the width of Cu nanoclusters on the clean surface, but a substantial difference in height is observed for Cu nanoclusters on the hydroxylated surface. As illustrated in the graph in Figure 4c, the most frequently occurring value for Cu cluster height is close to 0.4 ± 0.1 nm, indicating the formation of nanoclusters with no more than two layers of Cu. By using these values and the same procedure (eq 2) for the calculation of W_{adh} for the strongly hydroxylated surface, a higher adhesion energy is found for the Cu nanoclusters (W_{adh} = 3.55 ± 0.2 J/m^2). This value reflects a stronger binding of

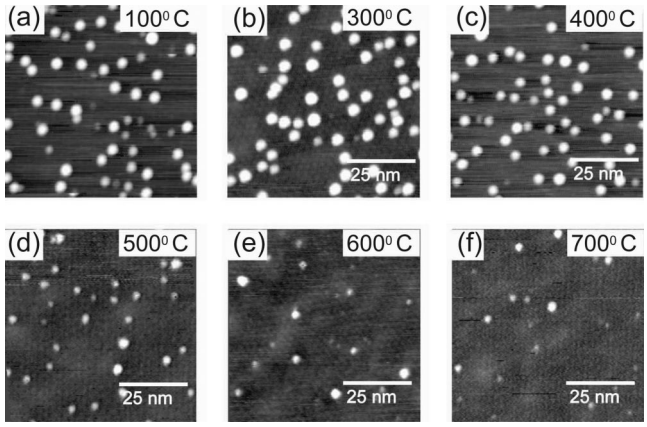

Figure 5. (a−f) High-resolution SFM images of Cu nanoclusters demonstrating the accumulated effect of stepwise heating (3 min at each temperature followed by cooling to RT and subsequent imaging) in the range of 100−700 °C. The initial coverage was ∼0.25 ML.

Cu and, thus, an increased wetting as evidenced by the decrease in cluster height. Although the exact geometry of the Cu bonding to the substrate is not resolved from our studies, the only option to increase the work of adhesion seems to be through the formation of Cu−O−Al bonding to the substrate, and we propose that this is the case here. The bonding of Cu atoms directly to a surface hydroxyl on Al_2O_3 is predicted in density functional theory (DFT) studies to be much weaker (W_{adh} = 0.87 J/m^2) than to Al or O−Al.[45] Starting from the "hydroxylated" surface, a strong Cu−O−Al bond may be formed by exchange of the H with Al and subsequent desorption of H_2(g).[28] We note, however, that the W_{adh} calculated from the experiment is much lower than the theoretical estimate for W_{adh} on a completely oxygen terminated (O−Al_2O_3(0001)) (W_{adh} =6.18 J/m^2), which would imply complete wetting of Cu. Such a condition is obviously not obtained under the conditions of our experiment, and we therefore assume that bonding of the Cu nanocluster achieved by deposition on the strongly hydroxylated surface (Figure 4b) may occur on a complex mixture of O, OH, and Al bonding sites. The existence of oxidized Cu (formally charged as +1) present in the form of Cu−O−Al links underneath the clusters can in principle be determined by an analysis of the X-ray excited (LMM) Auger transition of Cu.[27] Using our XPS setup, we performed a similar study of Cu, but because of rather low intensities from the 0.25 ML Cu, it was not possible to resolve the peak structure and unambiguously prove or rule out the existence of Cu^+ species in the present experiment.

D. Thermal Stability of Cu Nanoclusters on Clean and Hydroxylated Al_2O_3(0001). To gain further insight into the differences between the Al-terminated and strongly hydroxylated Al_2O_3 surfaces and shed more light on the bonding nature of the Cu nanoclusters to the substrate, we further investigated the thermal stability and morphology of the Cu/Al_2O_3 system in an extensive series of SFM images recorded after heating to temperatures in the interval from room temperature up to 700 °C. The data in Figure 5 illustrates examples of room temperature images recorded of Cu on the clean surface and shows the accumulated effect of heating the same sample for 3 min at every designated temperature. Similar data were also recorded and analyzed for the Cu nanoclusters on the strongly hydroxylated surface. Figure 6a−d represents plots of the density, coverage, and Cu nanocluster dimensions for the clean (black squares) and strongly hydroxylated Al_2O_3 substrates (circles) estimated from a statistical analysis of the Cu nanoclusters (most frequent values) as done in the previous sections. The temperature series demonstrate several surprising findings. First of all, for Cu deposited on the clean Al_2O_3 surface, the Cu remains dispersed as nanoclusters until Cu disappears from the surface at higher temperatures. The plot of the cluster density in Figure 6a illustrates this in quantitative detail. Above 300 °C, we start to see significant changes in the cluster morphologies compared with the equilibrium structures analyzed in the previous sections, and surprisingly, the decrease in cluster density (Figure 6a) initiated around 450 °C is not attributed to sintering, which would be expected, since also the total coverage estimated by the total Cu cluster volume (Figure 6b) clearly decreased. A typical sintering scenario would favor the growth of larger clusters at the expense of smaller clusters at a constant coverage, but instead, we observe that Cu disappears from the surface region. The gradual depletion of Cu from the surface layer is also observed in the XPS spectra of the Cu deposited surface taken after different temperatures of post-deposition heating (Figure 2b), where the Cu (2p) signal intensity decreases accordingly at higher temperatures, indicating that the Cu simply desorbs from the surface region. The same qualitative scenario is seen for the Cu nanoclusters deposited on the strongly hydroxylated surface, but interestingly, the process is delayed by more than 100 °C, indicative of a stronger initial cluster−substrate binding. It is seen from Figure 6a that the cluster density on the strongly hydroxylated surface in the low-temperature regime (100−300 °C) increased slightly by 15% compared with that of Cu on the clean surface, reflecting that the average cluster volume decreased and the density increased for a constant initial Cu coverage. Further, the general trend for the evolution of the Cu nanocluster density is similar, whereas a significant difference in the coverage is detected around 450 to 600 °C. A detailed comparison of the cluster dimension as a function of temperature shows that for both systems there is a gradual decrease of the cluster height toward one atomic layer of Cu (Figure 1c), but for the clean surface, the width (Figure 1d) decreases significantly, whereas for the hydroxylated surface, the cluster width remains approximately the same, indicating a disk-like Cu cluster. We attribute this finding to the existence of stabilizing Cu−O−Al bonding in the interface region for Cu nanoclusters grown on the strongly hydroxylated surface.

The melting point of bulk Cu is 1084 °C, which, at first hand, would rule out sublimation of Cu atoms to account for the loss of Cu seen for both systems above ∼450 °C and ∼550 °C, respectively. However, it is well-known that metallic nanoparticles may exhibit significant changes in their thermo-physical behavior compared with that in the bulk phase, and a number of studies have shown that the melting temperature deviates from the bulk value and becomes a size-dependent property.[49] Typically, the lowering effect of the melting point is attributed to a lowering of the average cohesive energy of the cluster due to the increased fraction of atoms placed on the surface,[50,51] and given that a typical 3.2 nm wide and 3 layer high Cu nanocluster (like those in Figure 1b) contains approximately 400 atoms, of which more than 40% are placed on the surface, we explain our findings in terms of a size variation in the desorption energy of Cu from a nanocluster. In fact, Wu et al. previously observed a significant downshift of the desorption temperature of Cu as a function of coverage in temperature programmed desorption (TPD) studies of Cu on a Al_2O_3/Mo(100) thin film substrate, and for coverages comparable to those in our study, Cu desorption was seen at temperature well-below 700 °C.[52] A second loss channel could be due to Cu diffusion into the bulk with the possibility of Cu aluminate

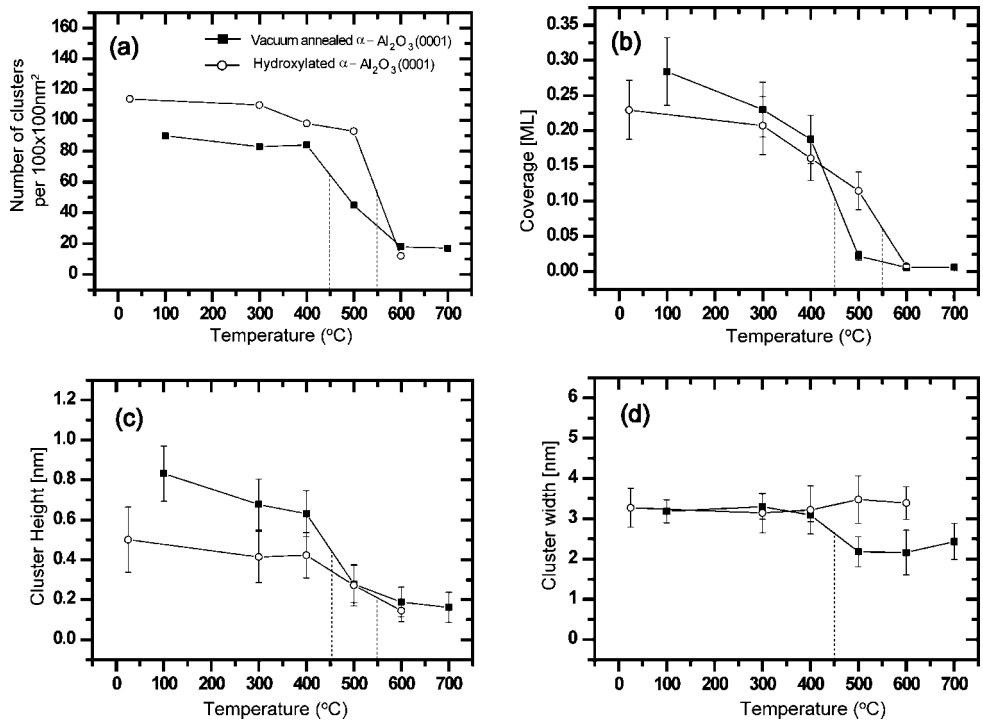

Figure 6. Cu nanocluster statistics estimated from SFM images as a function of temperature for the clean Al_2O_3 surface (■) and strongly hydroxylated surface (○). (a) Number of nanoclusters per 100 × 100 nm^2. (b) The coverage in monolayers of Cu (ML) estimated from the volume of Cu clusters in SFM images and 2D packing density of Cu. Errors were calculated from the uncertainties of the volume measurement. (c) Nanocluster height. (d) Nanocluster width. The height and width values in b and c and their variation represent the average value and variation obtained from a Gaussian fit to the actual measured statistical distribution. Vertical lines reflect the transition temperatures discussed in the text.

($CuAl_2O_4$) formation in an exchange reaction with surface Al. Diffusion into the bulk would imply a significant change in the substrate structure. However, it is clearly seen both on the hydroxylated and on the clean substrates (e.g., Figure 4d−f) that the large hexagonal lattice associated with the $\sqrt{31} \times \sqrt{31}R° \pm 9$ reconstruction is preserved without distortion at higher temperatures, indicating that the alumina surface layers are largely unaffected. To further rule out diffusion, we performed a simple XPS depth profile characterization using sequential sputtering at energies starting from 2 KeV to 5 KeV (15 min, Ar^+) followed by XPS analysis after each sputtering cycle. No Cu(2p) was detected in the XPS spectra. In addition, similar high-resolution SFM experiments on a different metal oxide $MgAl_2O_4$(001)[53] showed that Cu nanoclusters with a similar size disappeared from this surface at a comparable temperature, and given that migration of Cu in $MgAl_2O_4$ is probably more difficult than that in Al_2O_3,[54] we attribute the loss of Cu at higher temperatures to sublimation only.

The finding that Cu desorption is pronounced even at rather low temperature may have interesting implications for the sintering behavior of Cu nanocrystallites deposited on metal-oxide substrates in general. Basically, sintering is explained in terms of Ostwald ripening, if particle migration is not pronounced. In a ripening process, the metal atom is considered leaving the initial cluster in a thermally activated process and migrates to and joins a nearby metal cluster. On average, larger clusters will grow bigger at the expense of the smaller clusters. The sintering rate thus depends on the rate at which Cu atoms detach from the initial cluster and the diffusion rate involved in the migration of either single atoms or complexes to another cluster. Campbell et al. recently studied the significant implications of a cluster size variation in the free energy (i.e., atom detachment energy) of the sintering kinetics and concluded that sintering depends strongly on the cluster size and may be initiated at a much lower temperature than predicted from macroscopic properties.[55,56] Our results show that the rate of detachment must be significant even at low temperatures for the small Cu nanoclusters, and the size of the Cu nanoclusters should thus be taken into account when modeling the long-term sintering behavior. It is, however, quite surprising that the process leading to the final desorption of Cu from the surface seems to dominate over the situation where Cu atoms migrate over the surface and become imbedded in another cluster. The balance between both processes depends on the direct bonding strength of Cu atoms to the Al-terminated Al_2O_3(0001) surface, which is obviously quite weak, and the distance between individual clusters. At higher Cu coverage, it is likely that the migration distance between nanoclusters may be lowered sufficiently to activate pronounced sintering instead of desorption, and our future studies of the Cu/Al_2O_3 system will be aimed at studying the effect of coverage beyond the 0.25 ML used in this study. A second point to note is that the substrate on which Cu atoms diffuse for the clean and initially "hydroxylated" substrate is essentially the same at high temperature, since the $\sqrt{31} \times \sqrt{31}R \pm °9$ reconstructed state is regained after heating above 350 °C, and the slightly higher thermal stability of Cu on the latter substrate is therefore primarily considered to be an effect of the Cu−O−Al bonding and associated change in cluster morphology rather than a change in the diffusion rate on the substrate.

IV. Conclusions

We have used high-resolution scanning force microscopy (SFM) to obtain new detailed insight into the morphology of Cu nanoclusters supported on both clean and hydroxylated Al_2O_3(0001) substrates. For each substrate, we have analyzed a large number of Cu nanoclusters imaged by the SFM and

extracted values for the cluster height and width, and a comparative statistical analysis shows that hydroxylation influences the equilibrium morphology of the Cu nanoclusters. By means of the SFM, we could resolve a hexagonal shape of the Cu cluster top facet most likely reflecting a Cu(111) layer, and using this insight in combination with the measured cluster dimension, we could extract values for the work of adhesion for both the clean and the hydroxylated surfaces to be $W_{adh} = 3.32$ and $W_{adh} = 3.55$ J/m^2, respectively. The main conclusion is therefore that pre-exposing α-Al_2O_3 to water leads to increased Cu wetting, possibly because of the formation of Cu−O−Al bonds. This scenario is similar to the situation for Au nanoclusters on rutile $TiO_2(110)$,[57] where the presence of O species was found to stabilize Au nanoparticles, but it is opposite to Cu on ZnO where it is generally considered that a large concentration of oxygen vacancies lead to pronounced wetting of Cu, as directly observed in a reducing atmosphere.[4,58] The prehydroxylation of Al_2O_3 in this case is also seen to have some impact on the thermal stability of the clusters. Furthermore, the SFM studies of the Cu cluster density and size at different post deposition annealing reveal an onset for Cu desorption from the surface even at 450 °C, whereas for Cu supported on the prehydroxylated surface, the onset is shifted ∼100 °C higher. We attribute the stabilizing effect to the formation of Cu−O−Al bonds at the interface between the Cu and the Al_2O_3. The unusually low desorption temperatures observed in general may be related to the fact that the Cu nanoclusters in this study were very small, which is known to lead to significant changes in the atomic bonding strength, and we conclude that this effect may be more important in sintering studies and modeling of Cu diffusion for dispersed systems than normally considered.

Acknowledgment. The iNANO groups gratefully acknowledge financial support for the SFM and XPS systems from Haldor Topsøe A/S and the Lundbeck Foundation. J.V.L. furthermore acknowledges financial support from the Carlsberg Foundation.

References and Notes

(1) Handbook of Heterogeneous Catalysis; Ertl, G.; Knözinger, H.; Weitkamp, J., Eds.; *VCH:* Weinheim, 1997; Vol. 1−5.
(2) Henrich, V. E.; Cox, P. A. *The surface science of metal oxides*; Cambridge University Press: Cambridge, 1996.
(3) Weitkamp, J. In *Hydrocracking and Hydrotreating*; Ward, J. W.; Qader, S. A., Eds.; American Chemical Society: Washington D.C., 1975; Vol. 20, pp 1−27.
(4) Hansen, P. L.; Wagner, J. B.; Helveg, S.; Rostrup-Nielsen, J. R.; Clausen, B. S.; Topsøe, H. *Science* **2002**, *295*, 2053–2055.
(5) Costa, D.; Arrouvel, C.; Breysse, M.; Toulhoat, H.; Raybaud, P. *J. Catal.* **2007**, *246*, 325–343.
(6) Wang, J. G.; Hammer, B. *Top. Catal.* **2007**, *44*, 49–56.
(7) Molina, L. M.; Hammer, B. *Phys. Rev. Lett.* **2003**, 90.
(8) Worren, T.; Hansen, K. H.; Lægsgaard, E.; Besenbacher, F.; Stensgaard, I. *Surf. Sci.* **2001**, *477*, 8–16.
(9) Bäumer, M.; Freund, H.-J. *Prog. Surf. Sci.* **1999**, *61*, 127–198.
(10) Becker, C.; Rosenhahn, A.; Wiltner, A.; von Bergmann, K.; Schneider, J.; Pervan, P.; Milun, M.; Kralj, M.; Wandelt, K. *New J. Phys.* **2002**, 4.
(11) Schmid, M.; Kresse, G.; Buchsbaum, A.; Napetschnig, E.; Gritschneder, S.; Reichling, M.; Varga, P. *Phys. Rev. Lett.* **2007**, 99.
(12) Kresse, G.; Schmid, M.; Napetschnig, E.; Shishkin, M.; Kohler, L.; Varga, P. *Science* **2005**, *308*, 1440–1442.
(13) Sterrer, M.; Risse, T.; Heyde, M.; Rust, H. P.; Freund, H. J. *Phys. Rev. Lett.* **2007**, 98.
(14) Morita, S.; Wiesendanger, R.; Meyer, E. *Noncontact atomic force microscopy*; Springer: New York, 2002.
(15) Pang, C. L.; Raza, H.; Haycock, S. A.; Thornton, G. *Surf. Sci.* **2000**, *460*, L510−L514.
(16) Tait, S. L.; Ngo, L. T.; Yu, Q. M.; Fain, S. C.; Campbell, C. T. *J. Chem. Phys.* **2005**, 122.
(17) Barth, C.; Henry, C. R. *Nanotech.* **2004**, *15*, 1264–1272.
(18) Barth, C.; Pakarinen, O. H.; Foster, A. S.; Henry, C. R. *Nanotech.* **2006**, *17*, S128−S136.
(19) Ilinich, O.; Ruettinger, W.; Liu, X. S.; Farrauto, R. *J. Catal.* **2007**, *247*, 112–118.
(20) Hansen, J. B. In *Handbook of Heterogeneous Catalysis*; Ertl, G.; Knözinger, H.; Weitkamp, J., Eds.; VCH: Weinheim, 1997; Vol. 4, pp 1856−1876.
(21) Klier, K. *Adv. Catal.* **1982**, *31*, 243–313.
(22) Nakamura, J.; Choi, Y.; Fujitani, T. *Top. Catal.* **2003**, *22*, 277–285.
(23) Henry, C. R. *Surf. Sci. Rep.* **1998**, *31*, 231–325.
(24) Bäumer, M.; Freund, H. J. *Prog. Surf. Sci.* **1999**, *61*, 127–198.
(25) Chambers, S. A.; Droubay, T.; Jennison, D. R.; Mattsson, T. R. *Science* **2002**, *297*, 827–831.
(26) Eng, P. J.; Trainor, T. P.; Brown, G. E.; Waychunas, G. A.; Newville, M.; Sutton, S. R.; Rivers, M. L. *Science* **2000**, *288*, 1029–1033.
(27) Niu, C.; Shepherd, K.; Martini, D.; Tong, J.; Kelber, J. A.; Jennison, D. R.; Bogicevic, A. *Surf. Sci.* **2000**, *465*, 163–176.
(28) Sanz, J. F.; Hernandez, N. C. *Phys. Rev. Lett.* **2005**, 94.
(29) Wang, X.-G.; Chaka, A.; Scheffler, M. *Phys. Rev. Lett.* **2000**, *84*, 3650–3653.
(30) Wulff, G. *Zeitschift der Kristallographie* **1901**, *34*, 449–530.
(31) Hansen, K. H.; Worren, T.; Stempel, S.; Lægsgaard, E.; Bäumer, M.; Freund, H.-J.; Besenbacher, F.; Stensgaard, I. *Phys. Rev. Lett.* **1999**, *83*, 4120–4123.
(32) Lauritsen, J. V.; Christensen, M. C.; Venkataramani, K.; Hinnemann, B.; Helveg, S.; Clausen, B. S.; Besenbacher, F. , in preparation, 2008.
(33) French, T. M.; Somorjai, G. A. *J. Phys. Chem.* **1970**, *74*, 2489-&
(34) Renaud, G.; Villette, B.; Vilfan, I.; Bourret, A. *Phys. Rev. Lett.* **1994**, *73*, 1825–1828.
(35) Wang, J.; Howard, A.; Egdell, R. G.; Pethica, J. B.; Foord, J. S. *Surf. Sci.* **2002**, *515*, 337–343.
(36) Kelber, J. A. *Surf. Sci. Rep.* **2007**, *62*, 271–303.
(37) Barth, C.; Reichling, M. *Nature* **2001**, *414*, 54–57.
(38) Pakarinen, O. H.; Barth, C.; Foster, A. S.; Henry, C. R. *J. Appl. Phys.* **2008**, 103.
(39) Højrup-Hansen, K. Ph.D. Thesis, University of Aarhus, 2001.
(40) Vitos, L.; Ruban, A. V.; Skriver, H. L.; Kollar, J. *Surf. Sci.* **1998**, *411*, 186–202.
(41) Barth, C.; Reichling, M. *Nature* **2001**, *414*, 54–57.
(42) Wang, J.; Howard, A.; Egdell, R. G.; Pethica, J. B.; Foord, J. S. *Surf. Sci.* **2002**, *515*, 337–343.
(43) Lodziana, Z.; Nørskov, J. K.; Stoltze, P. *J. Chem. Phys.* **2003**, *118*, 11179–11188.
(44) Toofan, J.; Watson, P. R. *Surf. Sci.* **1998**, *401*, 162–172.
(45) Lodziana, Z.; Nørskov, J. K. *J. Chem. Phys.* **2001**, *115*, 11261–11267.
(46) Barth, C.; Reichling, M. In *Noncontact Atomic Force Microscopy*; Morita, S.; Wiesendanger, R.; Meyer, E., Eds.; Springer Verlag: Berlin, 2002; pp 135−145.
(47) Trevethan, T.; Kantorovich, L. *Nanotech.* **2006**, *17*, S205−S212.
(48) Wefers, K.; Chanakya, M. *Oxides and Hydroxides of Aluminum, Alcoa Laboratories*, 1987.
(49) Wronski, C. R. M. *British J. Appl. Phys.* **1967**, *18*, 1731.
(50) Safaei, A.; Shandiz, M. A.; Sanjabi, S.; Barber, Z. H. *J. Phys.: Condens. Matter* **2007**, 19.
(51) Puri, P.; Yang, V. *J. Phys. Chem. C* **2007**, *111*, 11776–11783.
(52) Wu, M. C.; Oh, W. S.; Goodman, D. W. *Surf. Sci.* **1995**, *330*, 61–66.
(53) Rasmussen, M. K.; Lauritsen, J. V.; Besenbacher, F.,unpublished results.
(54) Sehested, J.; Gelten, J. A. P.; Helveg, S. *Appl. Catal., A* **2006**, *309*, 237–246.
(55) Campbell, C. T.; Parker, S. C.; Starr, D. E. *Science* **2002**, *298*, 811–814.
(56) Parker, S. C.; Campbell, C. T. *Phys. Rev. B* **2007**, 75.
(57) Matthey, D.; Wang, J. G.; Wendt, S.; Matthiesen, J.; Schaub, R.; Lægsgaard, E.; Hammer, B.; Besenbacher, F. *Science* **2007**, *315*, 1692–1696.
(58) Grunwaldt, J.-D.; Molenbroek, A. M.; Topsøe, N.-Y.; Topsøe, H.; Clausen, B. S. *J. Catal.* **2000**, *194*, 452–460.
(59) Gritschneder, S.; Namai, Y.; Iwasawa, Y.; Reichling, M. *Nanotech.* **2005**, *16*, S41–S48.

JP804492H